

Article

Microwave-Assisted Solvothermal Synthesis of Chalcogenide Composite Photocatalyst and Its Photocatalytic CO₂ Reduction Activity under Simulated Solar Light

Gang-Juan Lee¹, Yu-Hong Hou¹, Hsin-Ting Huang¹, Wenmin Wang², Cong Lyu² 
and Jerry J. Wu^{1,*} 

¹ Department of Environmental Engineering and Science, Feng Chia University, Taichung 407, Taiwan; gjlee@fcu.edu.tw (G.-J.L.); p56074034@gs.ncku.edu.tw (Y.-H.H.); M0702014@mail.fcu.edu.tw (H.-T.H.)

² College of New Energy and Environment, Jilin University, Changchun 130021, China; wangwm17@mails.jlu.edu.cn (W.W.); lvcong@jlu.edu.cn (C.L.)

* Correspondence: jjwu@mail.fcu.edu.tw; Tel.: +886-4-24517250 (ext. 5206)

Received: 17 June 2020; Accepted: 15 July 2020; Published: 15 July 2020



Abstract: A novel heterostructure consisting of Ru and Cu co-doped ZnS nanopowders (RCZS) into a MoS₂-graphene hybrid (MSG) is successfully prepared by the microwave-assisted solvothermal approach. RCZS nanopowders are fabricated on the surface of MSG, which produces a nanoscale interfacial between RCZS and MSG. As the photo-excited electrons of RCZS can easily migrate to MoS₂ through graphene by hindering the electron and hole (e⁻ and h⁺) recombination, the photocatalytic activity could be improved by effective charge transfer. As RCZS are anchored onto the MSG, the photoluminescence intensity of the chalcogenide composite photocatalyst obviously decreases. In addition, a quaternary ruthenium and copper-based chalcogenide RCZS/MSG is able to improve the harvest and utilization of light. With the increase in the concentrations of Ru until 4 mol%, the band gap significantly decreases from 3.52 to 2.73 eV. At the same time, moderate modification by ruthenium can decrease the PL intensity compared to the pristine CZS/MSG sample, which indicates the enhancement of e⁻ and h⁺ separation by Ru addition. The photocatalytic activity of as-synthesized chalcogenide composite photocatalysts is evaluated by the photocatalytic carbon dioxide reduction. Optimized operation conditions for carbon dioxide reduction have been performed, including the concentration of NaOH solution, the amount of RCZS/MSG photocatalyst, and the content of co-doped ruthenium. The doping of ruthenium would efficiently improve the performance of the photocatalytic activity for carbon dioxide reduction. The optimal conditions, such as the concentration of 2 M NaOH and the 0.5RCZS/MSG dosage of 0.05 g L⁻¹, provide the maximum methane gas yield of 58.6 μmol h⁻¹ g⁻¹.

Keywords: chalcogenide; heterostructured photocatalyst; co-doping; carbon dioxide reduction

1. Introduction

As solar energy is a kind of environmentally friendly energy source, it is a great idea to convert solar energy into solar fuels via the photocatalytic reaction, i.e., the photocatalytic carbon dioxide reduction [1,2]. It is also a sustainable carbon circle approach to solve both the energy crisis and greenhouse effect issues via photocatalytic hydrogen evolution or photocatalytic CO₂ reduction [3–5]. There are two sorts of solar fuels: (1) Hydrogen (H₂)- and (2) carbon-based fuels, including carbon monoxide (CO), methane (CH₄), methanol (CH₃OH), ethanol (C₂H₅OH), formic acid (HCOOH), and formaldehyde (HCHO) [1,2,4]. The production of carbon-based fuels by the photocatalytic CO₂

reduction is a useful strategy to reduce CO₂ in the atmosphere due to the capturing and recycling of CO₂. However, CO₂ is a very stable molecule with extreme difficulty to chemically activate [2,6]. The single-electron reduction of CO₂ to form the radical CO₂^{•-} involves multiple electron processes, leading to the higher consumption of solar energy by the photocatalysis. Therefore, the best strategy to enhance the light harvesting is to create such a photocatalyst, which has not only a narrow band gap, but also the efficient separation of e⁻ and h⁺ pairs in the photocatalytic system. In addition, a quaternary copper-based chalcogenide performed efficient capture and utilization of solar energy [7–9]. Meanwhile, heterostructured photocatalysts possess a synergic effect to augment the photocatalytic activity [10,11]. MoS₂/graphene has been reported to have unique properties, such as large surface area, superior electron mobility, and excellent catalytic ability [7]. According to the references, many scientists have synthesized new heterostructured photocatalysts for exploring pronounced enhancements in photocatalytic performance [7–12].

Based on our previous studies, we know that copper-modified zinc sulfide could effectively enhance the photocatalytic activity efficiency [13,14]. Additionally, ruthenium addition could also create the acceptor energy levels to capture e⁻ from the valence band (VB), leading to a light harvesting efficiency from the ultraviolet light region to the visible light region [15]. On top of that, the active ruthenium and CO₂ possess a sensitive interaction, resulting in a higher selectivity to reduce CO₂ [16,17]. Ruthenium anchored onto graphene oxide (Ru-phen-GO) could produce methanol at 82.9 μmol h⁻¹ g⁻¹ [18]. Therefore, in this study, we have synthesized novel Ru and Cu co-doped ZnS nanopowders (RCZS)/MoS₂/graphene (MSG) heterostructured photocatalysts via the microwave-assisted solvothermal method to explore their photocatalytic performances in carbon dioxide reduction via simulated solar irradiation.

2. Results and Discussion

2.1. Chalcogenide Composite Photocatalysts

MoS₂-graphene has been reported to not only provide the reactive sites, but also enhance the e⁻ and h⁺ transfer [7,19]. Therefore, in this study, we attempted to add different amounts of the MSG hybrid to modify the ZnS photocatalyst. Figure 1a reveals the bare ZnS nanosphere with an average diameter of 113.7 nm. However, according to Figure 1b–d, the size of the ZnS particles decreased as the amount of MSG hybrid was increased from 0.1 wt.% to 1.0 wt.%. This clearly reveals that uniform structures of nanoparticles are well dispersed on exfoliated graphene nanosheets by the microwave-assisted solvothermal method, as shown in Figure 1(c1,d1). Moreover, MSG could increase the specific surface area of the samples from 72.91 to 104.60 m²/g by adding 0.5 wt.% MSG hybrid. Meanwhile, the charge transfer resistance was found to decrease from 6.19 to 5.07 Ω by adding 0.5 wt.% MSG hybrid. The photocurrent density was determined to slightly increase from 8.98 to 9.06 mA/cm² by adding 0.5 wt.% MSG hybrid due to the formation of heterostructured interfaces. However, excess interfaces, such as 1 wt.% MSG, would result in more grain boundaries for lowering the electron transportation. On the basis of the above results, we added a 0.5 wt.% MSG hybrid to conduct the next process.

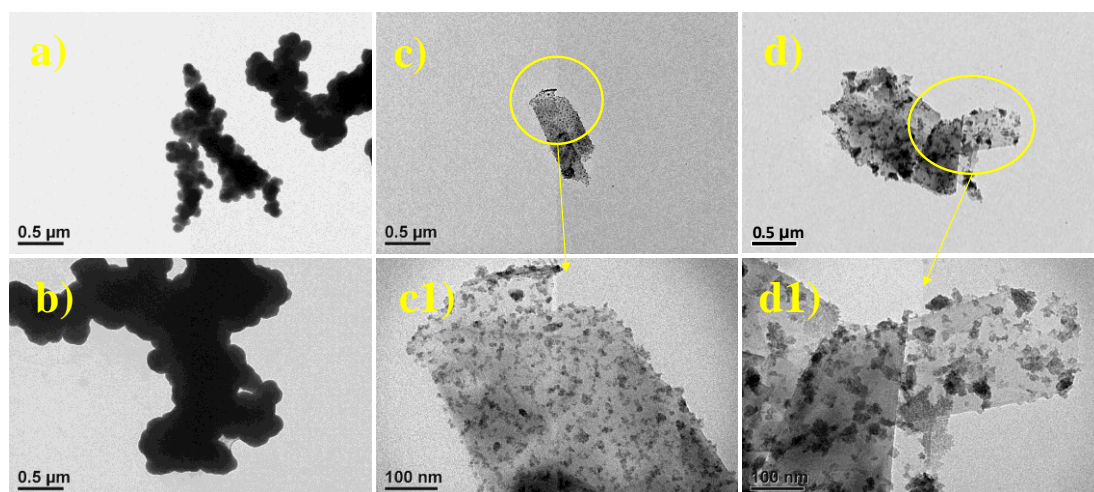


Figure 1. TEM images of as-synthesized ZnS photocatalysts with different amounts of MoS₂/graphene (MSG): (a) 0 wt.%, (b) 0.1 wt.%, (c) 0.5 wt.%, (c1) enlarged (c), (d) 1.0 wt.%, (d1) enlarged (d).

According to our previous study, we know that the doping of copper into ZnS would improve its photocatalytic activity more efficiently [20]. In addition, it shows the highest photocatalytic activity by 4 mol% copper addition. Therefore, 4 mol% copper doped into ZS/MSG was adopted in this study. Subsequently, we prepared the heterostructured photocatalysts, RCZS/MSG, via the doping of various amounts of ruthenium. The major peaks at 28.7°, 48.2°, and 57.0° pertain to (111), (220), and (311) planes of the cubic lattice of the ZnS phase (JCPDS card No. 05-0566), as shown in Figure 2. The average crystallite size of the as-synthesized ZnS nanoparticles, D_{111} , is 2.48 ± 0.032 nm. D_{50} of RCZS/MSG nanopowder is slightly decreased by doping ruthenium. The characteristics of the ruthenium-doped CZS/MSG nanoparticles are revealed in Table 1. The surface area decreases with the increase in ruthenium doping content from 46.23 to 35.90 m²/g due to the particle agglomeration in spite of the further slight increase in BET by doping more ruthenium up to 4%. In addition, the photocurrent density is 7.43 mA/cm² by doping 0.5 mol% ruthenium, which also has the highest percentage increase in photocurrent density (563.4%) than the other samples. A higher photocurrent density indicates that the photons absorbed by the photocatalyst can generate the photoexcited carriers efficiently. Therefore, the 0.5RCZS/MSG sample has outstanding photocatalytic activity. The band gap of pristine ZnS is 3.74 eV (data not shown). The band gap energy of RCZS/MSG nanopowder was calculated to redshift from 3.74 to 2.73 eV (Figure 3a), which can be assigned to ruthenium doping. Figure 3b indicates the conduction band (CB) and valence band (VB) edge positions of RCZS/MSG nanopowder. RCZS/MSG heterostructured photocatalysts possess a more negative potential than the reduction potential of the carbon dioxide level ($E = -0.24$ eV, CH₄/CO₂), leading to conversion from CO₂ to CH₄ [2]. Figure 4 reveals peaks at 360, 451, 469, 483, and 493 nm, and the intensity of the peaks declines by doping ruthenium due to the S vacancies, where surface defects can act as the adsorption sites to transfer e⁻ to the adsorbed species [21,22]. The emission band at 468–493 nm is due to the recombination of electrons in the sulfur vacancy level with the holes in the zinc vacancy (V_{Zn}) [21]. Therefore, the S vacancy could inhibit the e⁻ and h⁺ pair recombination and enhance the blue-indigo-violet emission by the modification of ruthenium, as shown in Figure 4b. In addition, moderate modification by ruthenium can decrease the PL intensity compared to that of the CZS/MSG sample, leading to the effective e⁻ and h⁺ pair separation. On the basis of the aforementioned discussion, we know that the new RCZS/MSG heterostructured photocatalysts could suitably improve the optical performance and enhance photocatalytic activity.

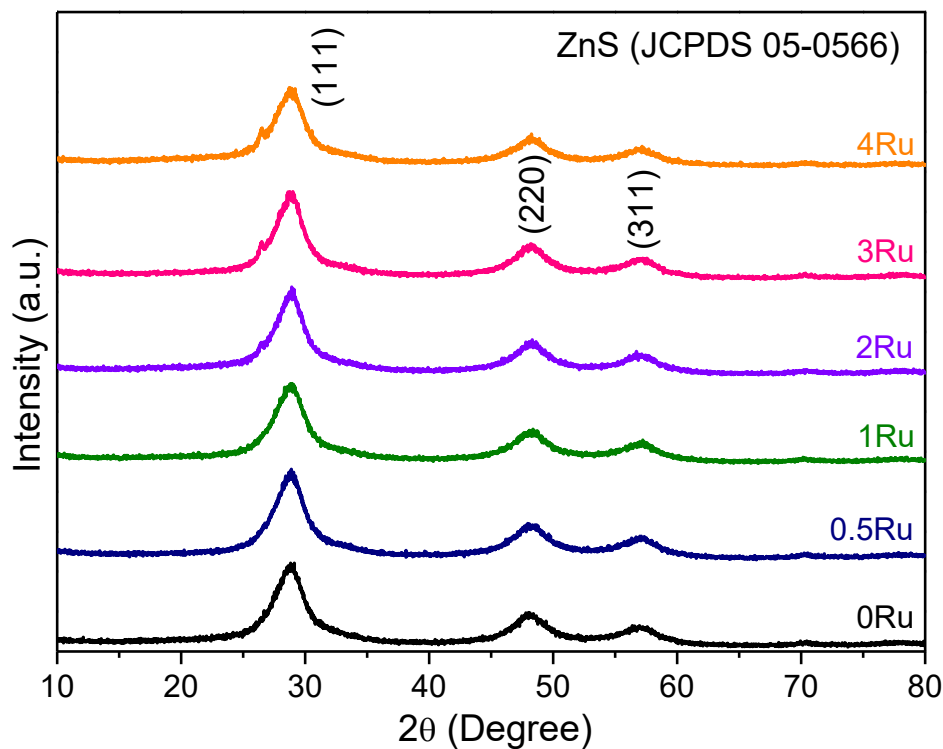


Figure 2. XRD patterns of ruthenium-doped CZS/MSG heterostructured photocatalysts.

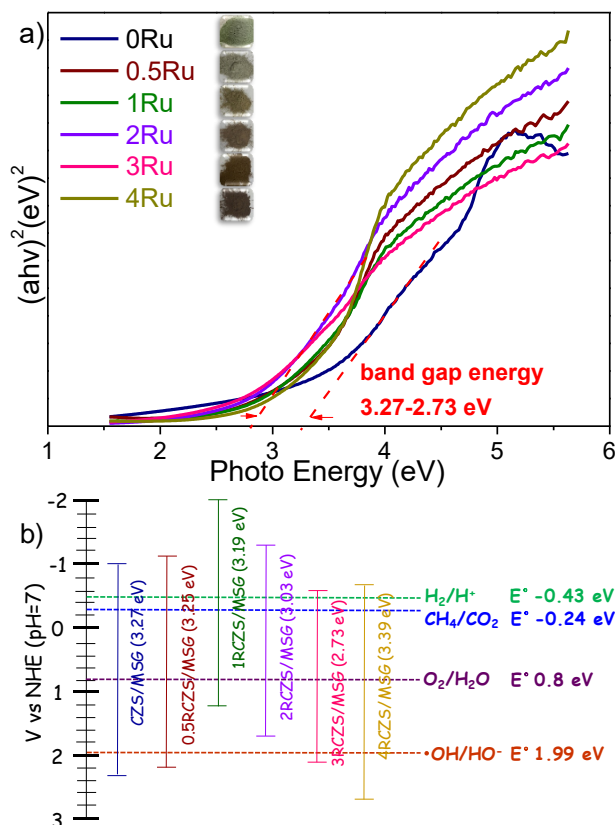
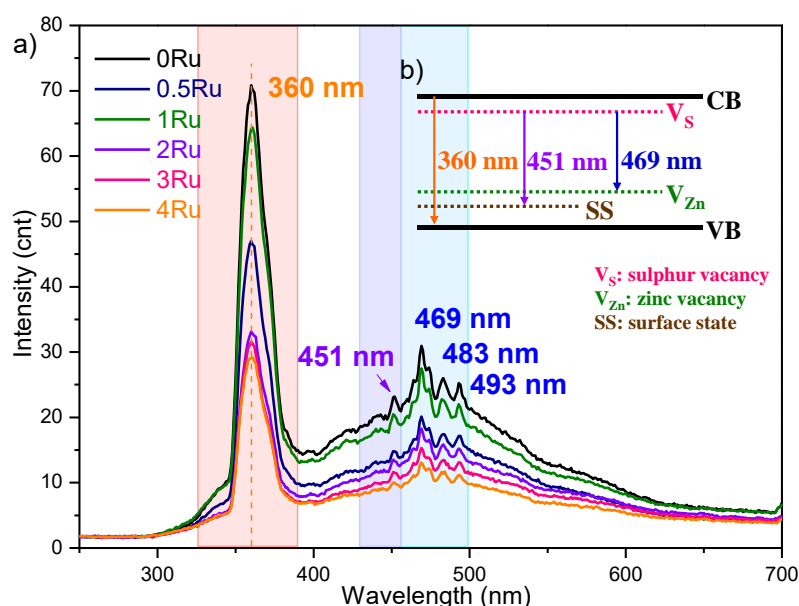


Figure 3. (a) UV-Vis absorption spectra of ruthenium-modified CZS/MSG heterostructured photocatalysts. Inset displays the digital camera photos for the corresponding photocatalysts. (b) Energy-level diagram revealing the conduction band (CB) and valence band (VB) edge positions of ruthenium-doped CZS/MSG heterostructured photocatalysts.

Table 1. Summary of average crystallite size D_{111} , particle size distribution D_{50} , BET, and photocurrent of as-synthesized CZS/MSG heterostructured photocatalysts with different amounts of ruthenium.

CZS/MSG	0.5Ru	1Ru	2Ru	3Ru	4Ru
D_{111} (nm) ¹	2.50	2.48	2.53	2.55	2.33
D_{50} (μm) ²	3.66	3.77	3.57	3.89	3.61
S_{BET} (m^2/g)	46.23	40.97	30.25	34.10	35.90
Pore size (\AA)	49.39	40.77	57.06	51.97	52.13
Pore volume (cm^3/g)	0.0571	0.0418	0.0432	0.0443	0.0468
Photocurrent density (mA/cm^2) ³	7.43	3.70	4.41	7.08	8.65
Dark current density (mA/cm^2)	1.12	1.93	1.64	2.52	3.27
percentage increase in current	563.4	91.7	168.9	181.0	164.5

¹ D_{hkl} is the particle size perpendicular to the normal line of the (hkl) plane. The average crystallite size of the as-synthesized semiconductor particles can be calculated using the Debye Scherrer's equation ($D_{\text{hkl}} = k\lambda/(\beta_{\text{hkl}}\cos\theta_{\text{hkl}})$).
² Particle size distribution D_{50} is the value of the particle diameter at 50% in the cumulative distribution. ³ The photocurrent density of samples obtained at 1.5 V vs. Ag/AgCl reference electrode in 0.1 M $\text{K}_4\text{F}(\text{CN})_6$ solution under UV light (8 W, $\lambda = 365$ nm).

**Figure 4.** (a) PL spectra, and (b) energy band diagram of ruthenium-doped CZS/MSG heterostructured photocatalysts.

2.2. Photocatalytic Carbon Dioxide Reduction

The photocatalytic carbon dioxide reduction activities of RCZS/MSG heterostructured photocatalysts were performed via simulated solar light. The experimental parameters, such as the different types of RCZS/MSG heterostructured photocatalyst, the concentration of reductant, and the dosages of 0.5RCZS/MSG, affecting the solar fuel evolution efficiency are evaluated below.

2.2.1. The Different Types of RCZS/MSG Heterostructured Photocatalyst

The formation of a heterojunction structure could improve the e^- and h^+ pair separation and photocatalytic reaction efficiency [7,23]. In addition, our previous research indicated that the CZS composite photocatalyst exhibited a lower methane generation rate ($2.9 \mu\text{mole h}^{-1} \text{g}^{-1}$) [20]. Therefore, we prepared the ruthenium and MSG-modified CZS to form the heterostructured photocatalyst, resulting in improved photocatalytic activity. First, the photolysis experiment was conducted and the result gave zero gas evolution, which means the mechanism by the direct photolysis can be negligible. Then, the addition of 0.5 wt.% MSG hybrid to the CZS composite photocatalyst slightly enhanced the methane generation rate from 2.9 to $12.4 \mu\text{mole h}^{-1} \text{g}^{-1}$. It may be that the presence of the MSG

hybrid cocatalyst can not only increase the e^- and h^+ pair separation efficiency, but also provide more catalytically active sites from MoS_2 [7]. Meanwhile, Figure 5a shows the photocatalytic reduction activity of carbon dioxide in NaOH solution over CZS/MSG by various Ru^{3+} ion amounts under 12 h illumination of simulated solar light. It can be seen that the co-doped 0.5 mol% ruthenium has the highest activity for solar fuel generation, such as methane ($23.4 \mu\text{mole h}^{-1} \text{g}^{-1}$) and hydrogen ($34.8 \mu\text{mole h}^{-1} \text{g}^{-1}$). The active ruthenium and CO_2 possess a sensitive interaction, resulting in the high selectivity to reduce CO_2 [16,17]. Furthermore, the high surface area of the photocatalyst favors better photocatalytic activity [24]. Therefore, we used the 0.5RCZS/MSG heterostructured photocatalyst to adjust the factors of photocatalytic activity in the next experimental procedure.

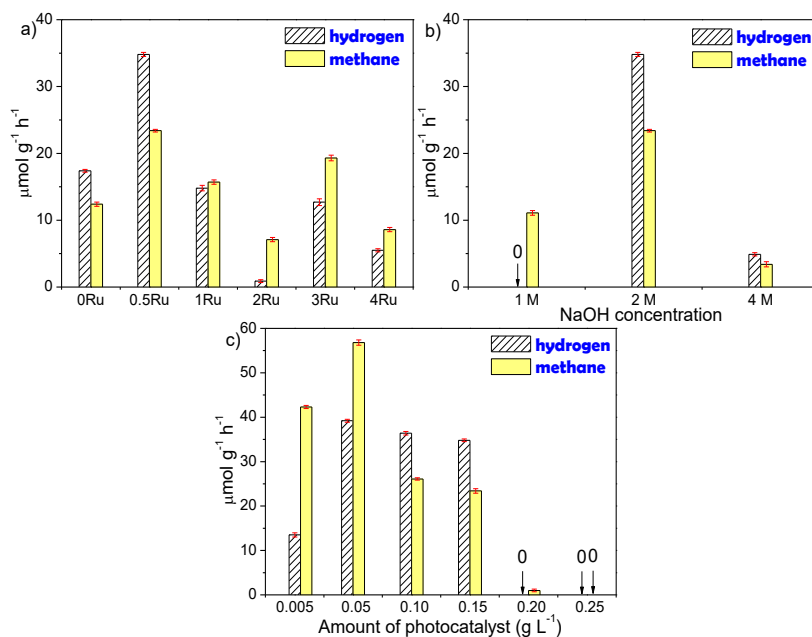


Figure 5. (a) Relation of the Ru doping amount to the photocatalytic carbon dioxide reduction (2 M NaOH, and 0.15 g L^{-1} photocatalyst dosage). (b) Relation of the concentration of reductant to the photocatalytic carbon dioxide reduction (0.15 g L^{-1} of 0.5 Ru and Cu co-doped ZnS nanopowders (RCZS)/MSG photocatalyst). (c) Relation of the content of 0.5RCZS/MSG photocatalyst to the photocatalytic carbon dioxide reduction (2 M NaOH).

2.2.2. The Concentration of Reductant

Caustic solution, NaOH, would increase the CO_2 solubility into water [25,26]. In addition, the hydroxyl ion (OH^-) can serve as a hole scavenger to enhance the e^- and h^+ pair separation efficiency [25]. Therefore, we prepared three NaOH concentrations to test the photocatalytic activity, as shown in Figure 5b. From the results, we know that the appropriate NaOH concentration at 2 M could perform with excellent photocatalytic activity.

2.2.3. The Dosages of 0.5RCZS/MSG

Figure 5c reveals the dosage influence ($0.005\text{--}0.25 \text{ g L}^{-1}$) on photocatalytic CO_2 reduction for 0.5RCZS/MSG in aqueous NaOH solution for 12 h irradiation. It has maximum solar fuel yields as high as $56.8 \mu\text{mole h}^{-1} \text{g}^{-1}$ methane and $39.2 \mu\text{mole h}^{-1} \text{g}^{-1}$ hydrogen at 0.05 g L^{-1} photocatalyst dosage. While the photocatalyst amount is below 0.05 g L^{-1} , the available active sites of the system decrease, resulting in the decrease in photocatalytic activity. On the contrary, as the photocatalyst amount is more than 0.05 g L^{-1} , the excess suspended catalysts could block or scatter the simulated solar light, leading to low photocatalytic efficiency. Moreover, the excess suspended catalysts could enhance the CO_2 adsorption by the catalyst, resulting in a decrease in free carbon dioxide in the solution,

giving lower methane production than hydrogen production. Therefore, the solar fuel production efficiency reduces above and below 0.05 g L^{-1} .

Based on the above results, Figure 6 shows the photocatalytic CO_2 reduction mechanism as proposed. The reduction half-reaction involves two pathways for the formation of methane and hydrogen via photocatalytic CO_2 reduction and water splitting reaction, as shown in Equations (1) and (2) [27]. Therefore, the photocatalytic system as reported herein allows the reduction of CO_2 at significant rates and the concomitant production of H_2 from water. According to the references, we know that dopants, ruthenium and copper, could increase the e^- and h^+ pair separation and migration, resulting in the enhanced photocatalytic efficiency [14,15]. The activated electrons can transfer to copper trap energy levels, allowing the activated electrons to transfer to the surface [13,14]. Additionally, the addition of ruthenium will create the acceptor energy levels to capture e^- from the VB, leading to better light harvesting efficiency extending from the ultraviolet light region to the visible light region [15]. In addition, the heterojunction structure can improve the e^- migration efficiency from ZnS to MoS_2 /graphene (belonging to interfacial charge transfer), reducing the e^- and h^+ pairs recombination [23]. Thus, the reaction rate could be improved by the effective charge transfer. The half reactions of the photocatalytic CO_2 reduction are indicated in Equations (1) and (3).

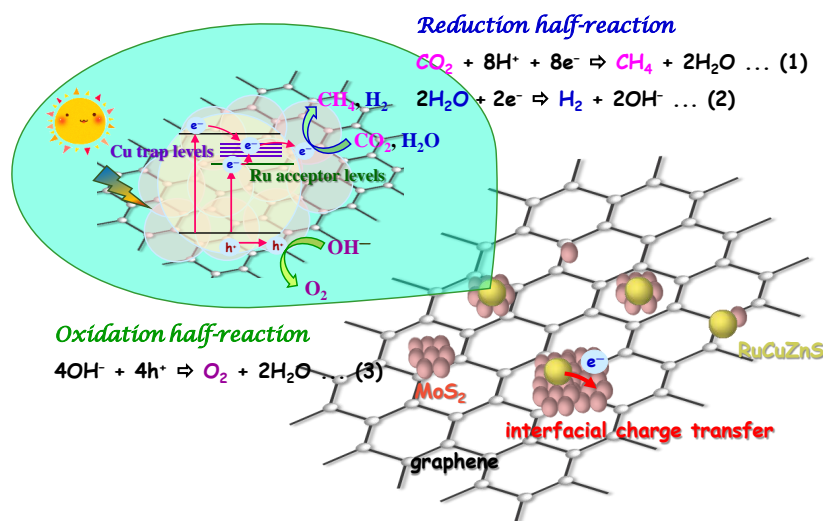


Figure 6. The photocatalytic CO_2 reduction mechanism over 0.5RCZS/MSG heterostructured photocatalysts.

3. Methods

3.1. Chalcogenide Composite Materials

3.1.1. MoS_2 /Graphene (MSG)

First, 0.1 M sodium molybdenum oxide dehydrate ($\text{Na}_2\text{MoO}_4 \cdot 2\text{H}_2\text{O}$, 98%, Alfa Aesar, Haverhill, MA, USA) and 0.22 M thioacetamide ($\text{C}_2\text{H}_5\text{NS}$, 99%, Merck, Darmstadt, Germany) were completely dissolved in deionized water (MoS_2 solution). Subsequently, 0.8 wt.% graphene (multi-layer graphene powder, Enerage, Yilan, Taiwan) was added into MoS_2 solution and heated using the microwave-assisted solvothermal method (2450 MHz, 1800 W, MARS 6, CEM). The operating conditions included 450 W, 160°C , and 20 min. The obtained MoS_2 /graphene hybrid powders were denoted as MSG.

3.1.2. ZnS Inlaid into MoS_2 /Graphene (ZS/MSG)

First, 0.5 M $\text{Zn}(\text{CH}_3\text{COO})_2 \cdot 2\text{H}_2\text{O}$ (99%, SHOWA, Tokyo, Japan) was added into the 30 mL solvent mixture [25 v/v% deionized water (DI) and 75 v/v% ethanol (EtOH)]. Then, 0.5 M $\text{C}_2\text{H}_5\text{NS}$, 1 wt.% citric acid monohydrate (CIT, $\text{C}_6\text{H}_8\text{O}_7 \cdot \text{H}_2\text{O}$, 99%, SHOWA, Tokyo, Japan) and 0–1.0 wt.% MSG were added into $\text{Zn}(\text{CH}_3\text{COO})_2$ solution and heated in the microwave instrument. Here, the operating conditions

were 450 W, 120 °C, and 20 min. Thus, we synthesized ZnS photocatalysts with different amounts of MSG, denoted as ZS/MSG.

3.1.3. Cu-Doped ZnS into MoS₂/Graphene (CZS/MSG)

Here, 0.5 M Zn(CH₃COO)₂•2H₂O was added into the 20 mL solvent mixture [25 v/v% DI water and 75 v/v% ethanol]. Then, 0.0671 g C₂H₅NS, 1 wt.% CIT, and 0.5 wt.% MSG were added into the Zn(CH₃COO)₂ solution (solution A). Next, 4 mol% Cu(CH₃COO)₂•H₂O (99%, Merck, Darmstadt, Germany) was added into the 10 mL solvent mixture (solution B). Subsequently, solution B was put into solution A and heated in the microwave instrument. Here, the operating conditions were 450 W, 120 °C, and 20 min. The obtained Cu-doped ZnS into MoS₂/graphene was denoted as CZS/MSG.

3.1.4. Ru, Cu co-Doped ZnS into MoS₂/Graphene (RCZS/MSG)

First, 0.5 M Zn(CH₃COO)₂•2H₂O was added into a 10 mL solvent mixture [25 v/v% DI water and 75 v/v% ethanol]. Then, 0.0671 g C₂H₅NS, 1 wt.% CIT, and 0.5 wt.% MSG were added into the Zn(CH₃COO)₂ solution (solution A). Next, 4 mol% Cu(CH₃COO)₂•H₂O was added into the 10 mL solvent mixture (solution B). Subsequently, 0.5–4 mol% ruthenium (III) chloride hydrate (RuCl₃•xH₂O, 99.9%, Alfa Aesar, Haverhill, MA, USA) was added into the 10 mL solvent mixture (solution C). Subsequently, solution B and solution C were put into solution A and heated in the microwave instrument. The obtained Ru, Cu co-doped ZnS into MoS₂/graphene was denoted as 0.5RCZS/MSG, 1RCZS/MSG, 2RCZS/MSG, 3RCZS/MSG, and 4RCZS/MSG, respectively.

3.2. Characterization Techniques

Transmission electron microscopy (TEM) images were recorded using a JEOL JEM-1400 model (Tokyo, Japan). BET (Brunauer-Emmett-Teller) surface area, D₅₀ (particle size distribution), XRD (X-ray diffraction), XPS (X-ray photoelectron spectroscopy), band gap, and PL (photoluminescence) were measured by a Micrometrics ASAP-2020 (Norcross, GA, USA), Shimadzu SALD-2300 (Tokyo, Japan), Rigaku Ultima III diffractometer (Tokyo, Japan), Physical Electronics PHI 5600 (Chanhassen, MN, USA), Shimadzu UV-2600 (Tokyo Japan), and Shimadzu RF-3501 spectrometer (Tokyo, Japan), respectively. The flat-band potential [14], charge transfer resistance, and photocurrent density were measured by the potentiostat/galvanostat PGSTAT302N, Metrohm Autolab (Herisau, Switzerland). The measurement of photocurrent density was conducted by adding 0.15 g as-synthesized catalyst into 0.5 mL Nafion solution (Type: DE-520) by ultrasound for 10 min, where 0.1 mL of the mixture solution was withdrawn and attached onto the 20 × 10 × 0.3 mm of indium tin oxide conductive glass (ITO). Then, the ITO conductive glass was dried overnight at room temperature under atmospheric conditions and employed as a working electrode. A Pt wire and Ag/AgCl electrode were used as the counter electrode and reference electrode, respectively. The photocurrent density measurement was performed in the 0.1 M K₄Fe(CN)₆ (99.9%, Sigma-Aldrich, St. Louis, MO, USA) electrolyte via an electrochemical workstation. In addition, a Pen-Ray lamp (8 W, λ = 365 nm; Model 11SC-1L; Series 90-0019-01; UVP, Cole-Parmer, Vernon Hills, IL, USA) was used as the light source.

3.3. Photocatalytic Hydrogen Evolution and Carbon Dioxide Reduction

The photocatalytic hydrogen evolution and carbon dioxide reduction were conducted by using 100 mL solution containing 1–4 M NaOH and 0–0.25 g L⁻¹ of ZnS composite photocatalysts in a single reactor. Subsequently, CO_{2(g)} was purged to dissolve in the solution for 10 min. The reactor was irradiated by a 350 W xenon light (KIT-XENON-ADJ350W) for 12 h, and the productions of hydrogen and methane gases were determined by GC-TCD (GC-2014, SHIMADZU (Tokyo, Japan), and China Chromatograph 8700T (Beijing, China)).

4. Conclusions

It is demonstrated that ruthenium co-doped CZS/MSG heterostructured photocatalysts act for the excellent photocatalysis of carbon dioxide reduction. The appropriate doping concentration of ruthenium could reach the maximum methane yield, where 0.5RCZ/MSG possesses outstanding physical and chemical properties, leading to the enhancement of the photocatalytic efficiency. In addition, ruthenium is a superior methanation cocatalyst. Therefore, the appropriate conditions, such as the concentration of 2 M NaOH and the photocatalyst dose of 0.05 g L⁻¹, could perform with better photocatalytic activity.

Author Contributions: Conceptualization, G.-J.L. and J.J.W.; methodology, all authors; formal analysis, G.-J.L. and Y.-H.H.; investigation, Y.-H.H., H.-T.H., and W.W.; writing—original draft preparation, G.-J.L.; writing—review editing and supervision, C.L. and J.J.W.; project administration, G.-J.L.; funding acquisition, J.J.W. All authors have read and agreed to the published version of the manuscript.

Funding: This research was funded by Ministry of Science and Technology (MOST), Taiwan.

Acknowledgments: The authors wish to thank for the financial support by the Ministry of Science and Technology (MOST) in Taiwan under the contract numbers of MOST-104-2221-E-035-004-MY3 and MOST-107-2221-E-035-001-MY3.

Conflicts of Interest: The authors declare no conflict of interest.

References

1. Low, J.; Cheng, B.; Yu, J. Surface modification and enhanced photocatalytic CO₂ reduction performance of TiO₂: A review. *Appl. Surf. Sci.* **2017**, *392*, 658–686. [[CrossRef](#)]
2. Nikokavoura, A.; Trapalis, C. Alternative photocatalysts to TiO₂ for the photocatalytic reduction of CO₂. *Appl. Surf. Sci.* **2017**, *391*, 149–174. [[CrossRef](#)]
3. Jiao, J.; Wei, Y.; Zhao, Z.; Zhong, W.; Liu, J.; Li, J.; Duan, A.; Jiang, G. Synthesis of 3D ordered macroporous TiO₂-supported Au nanoparticle photocatalysts and their photocatalytic performances for the reduction of CO₂ to methane. *Catal. Today* **2015**, *258*, 319–326. [[CrossRef](#)]
4. Chen, J.; Xin, F.; Qin, S.; Yin, X. Photocatalytically reducing CO₂ to methyl formate in methanol over ZnS and Ni-doped ZnS photocatalysts. *Chem. Eng. J.* **2013**, *230*, 506–512. [[CrossRef](#)]
5. Kortlever, R.; Balemans, C.; Kwon, Y.; Koper, M.T.M. Electrochemical CO₂ reduction to formic acid on a Pd-based formic acid oxidation catalyst. *Catal. Today* **2015**, *244*, 58–62. [[CrossRef](#)]
6. Gonell, F.; Puga, A.V.; Julián-López, B.; García, H.; Corma, A. Copper-doped titania photocatalysts for simultaneous reduction of CO₂ and production of H₂ from aqueous sulfide. *Appl. Catal. B Environ.* **2016**, *180*, 263–270. [[CrossRef](#)]
7. Ha, E.; Liu, W.; Wang, L.; Man, H.W.; Hu, L.; Tsang, S.C.E.; Chan, C.T.L.; Kwok, W.M.; Lee, L.Y.S.; Wong, K.Y. Cu₂ZnSnS₄/MoS₂-reduced graphene oxide heterostructure: Nanoscale interfacial contact and enhanced photocatalytic hydrogen generation. *Sci. Rep. UK* **2017**, *7*, 1–8. [[CrossRef](#)] [[PubMed](#)]
8. Lee, G.J.; Chen, H.C.; Wu, J.J. (In, Cu) Co-doped ZnS nanoparticles for photoelectrochemical hydrogen production. *Int. J. Hydrogen Energy* **2019**, *44*, 110–117. [[CrossRef](#)]
9. Lee, G.J.; Chen, H.C.; Wu, J.J. Enhancing the photocatalytic hydrogen evolution of copper doped zinc sulfide nanoballs through surfactants modification. *Int. J. Hydrogen Energy* **2019**, *44*, 30563–30573. [[CrossRef](#)]
10. Li, H.; Wang, Y.; Chen, G.; Sang, Y.; Jiang, H.; He, J.; Li, X.; Liu, H. Few-layered MoS₂ nanosheets wrapped ultrafine TiO₂ nanobelts with enhanced photocatalytic property. *Nanoscale* **2016**, *8*, 6101–6109. [[CrossRef](#)]
11. Luciani, G.; Imparato, C.; Vitiello, G. Photosensitive hybrid nanostructured materials: The big challenges for sunlight capture. *Catalysts* **2020**, *10*, 103. [[CrossRef](#)]
12. Yu, X.; Wang, L.; Zhang, J.; Guo, W.; Zhao, Z.; Qin, Y.; Mou, X.; Li, A.; Liu, H. Hierarchical hybrid nanostructures of Sn₃O₄ on N doped TiO₂ nanotubes with enhanced photocatalytic performance. *J. Mater. Chem. A* **2015**, *3*, 19129–19136. [[CrossRef](#)]
13. Lee, G.J.; Anandan, S.; Masten, S.J.; Wu, J.J. Sonochemical synthesis of hollow copper doped zinc sulfide nanostructures: Optical and catalytic properties for visible light assisted photosplitting of water. *Ind. Eng. Chem. Res.* **2014**, *53*, 8766–8772. [[CrossRef](#)]

14. Lee, G.J.; Anandan, S.; Masten, S.J.; Wu, J.J. Photocatalytic hydrogen evolution from water splitting using Cu doped ZnS microspheres under visible light irradiation. *Renew. Energy* **2016**, *89*, 18–26. [[CrossRef](#)]
15. Nosaka, Y.; Nishikawa, M.; Nosaka, A.Y. Spectroscopic investigation of the mechanism of photocatalysis. *Molecules* **2014**, *19*, 18248–18267. [[CrossRef](#)]
16. Kuriki, R.; Ishitani, O.; Maeda, K. Unique solvent effects on visible-light CO₂ reduction over ruthenium (II)-complex/carbon nitride hybrid photocatalysts. *ACS Appl. Mater. Inter.* **2016**, *8*, 6011–6018. [[CrossRef](#)]
17. Kwak, J.H.; Kovarik, L.; Szanyi, J. CO₂ reduction on supported Ru/Al₂O₃ catalysts: Cluster size dependence of product selectivity. *ACS Catal.* **2013**, *3*, 2449–2455. [[CrossRef](#)]
18. Kumar, P.; Sain, B.; Jain, S.L. Photocatalytic reduction of carbon dioxide to methanol using a ruthenium trinuclear polyazine complex immobilized on graphene oxide under visible light irradiation. *J. Mater. Chem. A* **2014**, *2*, 11246–11253. [[CrossRef](#)]
19. Yuan, Y.J.; Tu, J.R.; Ye, Z.J.; Chen, D.Q.; Hu, B.; Huang, Y.W.; Chen, T.T.; Cao, D.P.; Yu, Z.T.; Zou, Z.G. MoS₂-graphene/ZnIn₂S₄ hierarchical microarchitectures with an electron transport bridge between light-harvesting semiconductor and cocatalyst: A highly efficient photocatalyst for solar hydrogen generation. *Appl. Catal. B Environ.* **2016**, *188*, 13–22. [[CrossRef](#)]
20. Lee, G.J.; Hou, Y.H.; Liu, N.; Wu, J.J. Enhanced photocatalytic hydrogen and methane evolution using chalcogenide with metal ion modification via a microwave-assisted solvothermal method. *Catal. Today* **2019**. [[CrossRef](#)]
21. Wang, G.; Huang, B.; Li, Z.; Lou, Z.; Wang, Z.; Dai, Y.; Whangbo, M.H. Synthesis and characterization of ZnS with controlled amount of S vacancies for photocatalytic H₂ production under visible light. *Sci. Rep. UK* **2015**, *5*, 08544. [[CrossRef](#)] [[PubMed](#)]
22. Anila, E.I.; Safeera, T.A.; Reshmi, R. Photoluminescence of nanocrystalline ZnS thin film grown by sol-gel method. *J. Fluoresc.* **2015**, *25*, 227–230. [[CrossRef](#)] [[PubMed](#)]
23. Zhang, J.; Yu, J.; Zhang, Y.; Li, Q.; Gong, J.R. Visible light photocatalytic H₂-production activity of CuS/ZnS porous nanosheets based on photoinduced interfacial charge transfer. *Nano Lett.* **2011**, *11*, 4774–4779. [[CrossRef](#)] [[PubMed](#)]
24. He, Z.; Wen, L.; Wang, D.; Xue, Y.; Lu, Q.; Wu, C.; Chen, J.; Song, S. Photocatalytic reduction of CO₂ in aqueous solution on surface-fluorinated anatase TiO₂ nanosheets with exposed {001} facets. *Energy Fuel* **2014**, *28*, 3982–3993. [[CrossRef](#)]
25. Srinivas, B.; Shubhamangala, B.; Lalitha, K.; Kumar Reddy, P.A.; Kumari, V.D.; Subrahmanyam, M.; Ranjan, D.B. Photocatalytic reduction of CO₂ over Cu-TiO₂/molecular sieve 5A composite. *Photochem. Photobiol.* **2011**, *87*, 995–1001. [[CrossRef](#)]
26. Lingampalli, S.R.; Ayyub, M.M.; Rao, C.N.R. Recent progress in the photocatalytic reduction of carbon dioxide. *ACS Omega* **2017**, *2*, 2740–2748. [[CrossRef](#)]
27. Reli, M.; Šihor, M.; Kočí, K.; Praus, P.; Kozák, O.; Obalová, L. Influence of reaction medium on CO₂ photocatalytic reduction yields over ZnS-MMT. *GeoScience Eng.* **2012**, *58*, 34–42. [[CrossRef](#)]

